

000  
001  
002054  
055  
056

# Multi-channel Weighted Nuclear Norm Minimization for Real Color Image Denoising

057  
058  
059003  
004  
005  
006  
007060  
061  
062  
063

Anonymous ICCV submission

008  
009  
010  
011064  
065  
066

Paper ID 572

012  
013  
014067  
068  
069

## Abstract

015

070  
071

The noise structures among the R, G, B channels of real images are quite different due to the preprocessing steps in digital camera pipelines. This makes the real image denoising problem much more complex than traditional grayscale image denoising. In this paper, we propose a multi-channel optimization model for real color image denoising. Specifically, we introduce a weighting matrix into the data term to process adaptively each part of R, G, B channels in the joint patches concatenated by corresponding patches in these channels. In the regularization term, we employ the weighted nuclear norm to exploit the non-local self similar property. The proposed multi-channel weighted nuclear norm minimization (MC-WNNM) model is much more complex than the standard WNNM model. To solve this new problem, we reformulate the MC-WNNM model into a linear equality-constrained problem and solve it under the alternating direction method of multipliers (ADMM) framework. Each alternative updating step has closed-form solution and the convergence results are given. Experiments on benchmark datasets demonstrate that the proposed model outperforms state-of-the-art denoising methods on synthetic as well as real-world noisy images.

038  
039080  
081

## 1. Introduction

040  
041082  
083

Image denoising is an important problem in enhancing the image quality in computer vision systems. The traditional grayscale image denoising problem aims to recover the clean image  $\mathbf{x}$  from the noisy observation  $\mathbf{y} = \mathbf{x} + \mathbf{n}$ , where  $\mathbf{n}$  is often assumed to be additive white Gaussian noise (AWGN). Most image denoising methods in this field either employ the non-local self similarity (NSS) of natural images [1–7] or learn generative or discriminative denoisers from paired natural clean images and synthetic noisy images [8–12]. Among these methods, the weighted nuclear norm minimization (WNNM) method achieves excellent denoising performance by exploiting the NSS property

via low rank regularization.

The real color image denoising problem is not a trivial extension from single channel (grayscale image) to multiple channels (color image). The reason is that the noise in standard RGB (sRGB) space, though could be modeled as AWGN, are with different variances for different channels [13] due to the on-board processing steps in digital camera pipelines [14, 15]. This makes the real color image denoising problem much more complex. Directly applying the denoising methods for grayscale images to each channel of color images separately would obtain bad performance [16]. There are several work [14, 16–20] proposed specifically for color image denoising. The method [17] first transforms the color images into the luminance/chrominance space such as YCbCr before denoising, but this would make the noise distribution more complex in color images. The methods of [16, 20] process the joint patches concatenated by the corresponding patches in R, G, B channels and treat equally the patches in different channels. This would generate false colors or artifacts [16]. The methods of [14, 18, 19] ignore the non-local self similarity property of natural images, and their performance would be largely depressed [2, 7].

In order to deal with the R, G, B channels in color images more effectively, different noise properties of different channels should be considered in solving real color image denoising problem. Besides, due to its expressive denoising performance, the WNNM model [7] is employed to exploit the NSS property of natural images. In this paper, we proposed a multi-channel WNNM (MC-WNNM) model for real color image denoising. By introducing a weighting matrix to the WNNM model, the proposed MC-WNNM model no longer has closed-form solutions and more challenging to solve. By reformulating the proposed MC-WNNM model into a linear equality-constrained program with two variables, the relaxed problem can be solved under the alternating direction method of multipliers (ADMM) [21] framework. Each variable can be updated with closed-form solution [7, 22]. We also give the convergence results with detailed proof to guarantee a rational termination of the proposed algorithm.

108  
109  
110  
111  
112  
113  
114

## 2. Related Work

### 2.1. Weighted Nuclear Norm Minimization

As an extension to the nuclear norm minimization (NNM) model [23], the weighted nuclear norm minimization (WNNM) model [7] is described as

$$\min_{\mathbf{X}} \|\mathbf{Y} - \mathbf{X}\|_F^2 + \|\mathbf{X}\|_{\mathbf{w},*} \quad (1)$$

where  $\|\mathbf{X}\|_{\mathbf{w},*} = \sum_i w_i \sigma_i(\mathbf{X})$  is the weighted nuclear norm of matrix  $\mathbf{X}$ , and  $\mathbf{w} = [w_1, \dots, w_n]^\top$ ,  $w_i \geq 0$  is the weight vector,  $\sigma_i(\mathbf{X})$  is the  $i$ -th singular value of matrix  $\mathbf{X}$ . According to the Corollary 1 of [24], the problem (1) has closed-form solution if the weights are non-decreasing

$$\hat{\mathbf{X}} = \mathbf{U} \mathcal{S}_{\mathbf{w}/2}(\Sigma) \mathbf{V}^\top \quad (2)$$

where  $\mathbf{Y} = \mathbf{U} \Sigma \mathbf{V}^\top$  is the singular value decomposition [25] of  $\mathbf{Y}$  and  $\mathcal{S}_\tau(\bullet)$  is the generalized soft-thresholding operator with weight vector  $\mathbf{w}$ :

$$\mathcal{S}_{\mathbf{w}/2}(\Sigma_{ii}) = \max(\Sigma_{ii} - w_{ii}/2, 0) \quad (3)$$

Though having achieved excellent performance on grayscale image denoising, the WNNM model would generate false colors or artifacts [16], if being directly extended to real color image denoising by processing each channel separately or joint vectors concatenated by multiple channels. In this paper, for real noisy image denoising, we propose a multi-channel WNNM model which preserve the power of WNNM and be able to process the differences among different channels.

### 2.2. Real Color Image Denoising

During the last decade, several denoising methods are proposed for real color image denoising [17–20]. Among them, the CBM3D [17] first transform the RGB image into luminance-chrominance space (e.g., YCbCr) and then apply the famous BM3D method [2] on each channel separately with the patches being grouped only in the luminance channel. In [18], the authors proposed the “Noise Level Function” to estimate and remove the noise for each channel in natural images. However, the methods processing each channel separately would achieve inferior performance than processing jointly these channels [16]. The methods of [19, 20, 26] perform real color image denoising by concatenating the patches in R, G, B channels into joint vectors. However, the concatenation would treat each channel equally and ignore the different noise properties among these channels. The method in [14] models the cross-channel noise in real noisy image as a multivariate Gaussian and the noise is removed by the Bayesian nonlocal means filter [27]. The commercial software Neat Image [28] estimates the noise parameters from a flat region of the given noisy image and filters the noise correspondingly. But

these methods [14, 28] ignore the non-local self similarity property of natural images [2, 7].

In this paper, we introduce a weighting matrix which add different weights to different channels for color image denoising. The proposed multi-channel method can effectively solve the problem of different noise structures among different channels.

## 3. Color Image Denoising via Multi-channel Weighted Nuclear Norm Minimization

### 3.1. The Problem

The color image denoising problem is to recover the clean image  $\mathbf{x}_c$  from its noisy version  $\mathbf{y}_c = \mathbf{x}_c + \mathbf{n}_c$ , where  $c = \{r, g, b\}$  is the index of R, G, B channels and  $\mathbf{n}_c$  is the noise in  $c$ -th channel. Given a noisy color image  $\mathbf{y}_c$ , each local patch of size  $p \times p \times 3$  is extracted and stretched to a patch vector  $\mathbf{y} = [\mathbf{y}_r^\top \mathbf{y}_g^\top \mathbf{y}_b^\top]^\top \in \mathbb{R}^{3p^2}$ , where  $\mathbf{y}_r, \mathbf{y}_g, \mathbf{y}_b \in \mathbb{R}^{p^2}$  are corresponding patches in R, G, B, channels. For each local patch  $\mathbf{y}$ , we search the  $M$  most similar patches to it (including  $\mathbf{y}$  itself) by Euclidean distance in a  $W \times W$  local region around it. We stack the  $M$  similar patches column by column to form a noisy patch matrix  $\mathbf{Y} = \mathbf{X} + \mathbf{N} \in \mathbb{R}^{3p^2 \times M}$ , where  $\mathbf{X}$  and  $\mathbf{N}$  the corresponding clean and noise patch matrices.

According to [13], the noise in standard RGB (sRGB) space, though could be modeled as additive white Gaussian (AWGN), are with different variances for different channels. Therefore, it is problematic to directly apply denoising methods to the joint vectors concatenated by corresponding patches of the R, G, B channels. To validate this point, in Fig. 1, we show the clean image ‘‘kodim23’’ taken from the Kodak PhotoCD dataset, its degraded version generated by adding synthetic additive white Gaussian noise (AWGN) to each channel of ‘‘kodim23’’, and the denoised image by applying WNNM [7] on the joint vectors concatenated from R, G, B channels of the degraded image. The standard derivations of AWGN added to the R, G, B channels are  $\sigma_r = 40$ ,  $\sigma_g = 20$ ,  $\sigma_b = 30$ , respectively. The input standard derivation of the noise for the concatenated WNNM method is set as the Root Mean Square (RMS) of those in each channel, i.e.,  $\sigma = \sqrt{(\sigma_r^2 + \sigma_g^2 + \sigma_b^2)/3} = 31.1$ . From Fig. 1, one can see that the concatenated WNNM method treating each channel equally would remain some noise in the R and B channel, while over-smoothing the G channel of the degraded image. Hence, if the patches of different channels are treated adaptively in the concatenated vectors, the degraded color images would be recovered with better visual qualities.

In order to process each channel differently while still exploiting the joint structures of the color images, in this paper, we introduce a weighting matrix  $\mathbf{W}$  to the concatenated

162  
163  
164  
165  
166  
167  
168  
169  
170  
171  
172  
173  
174  
175  
176  
177  
178  
179  
180  
181  
182  
183  
184  
185  
186  
187  
188  
189  
190  
191  
192  
193  
194  
195  
196  
197  
198  
199  
200  
201  
202  
203  
204  
205  
206  
207  
208  
209  
210  
211  
212  
213  
214  
215

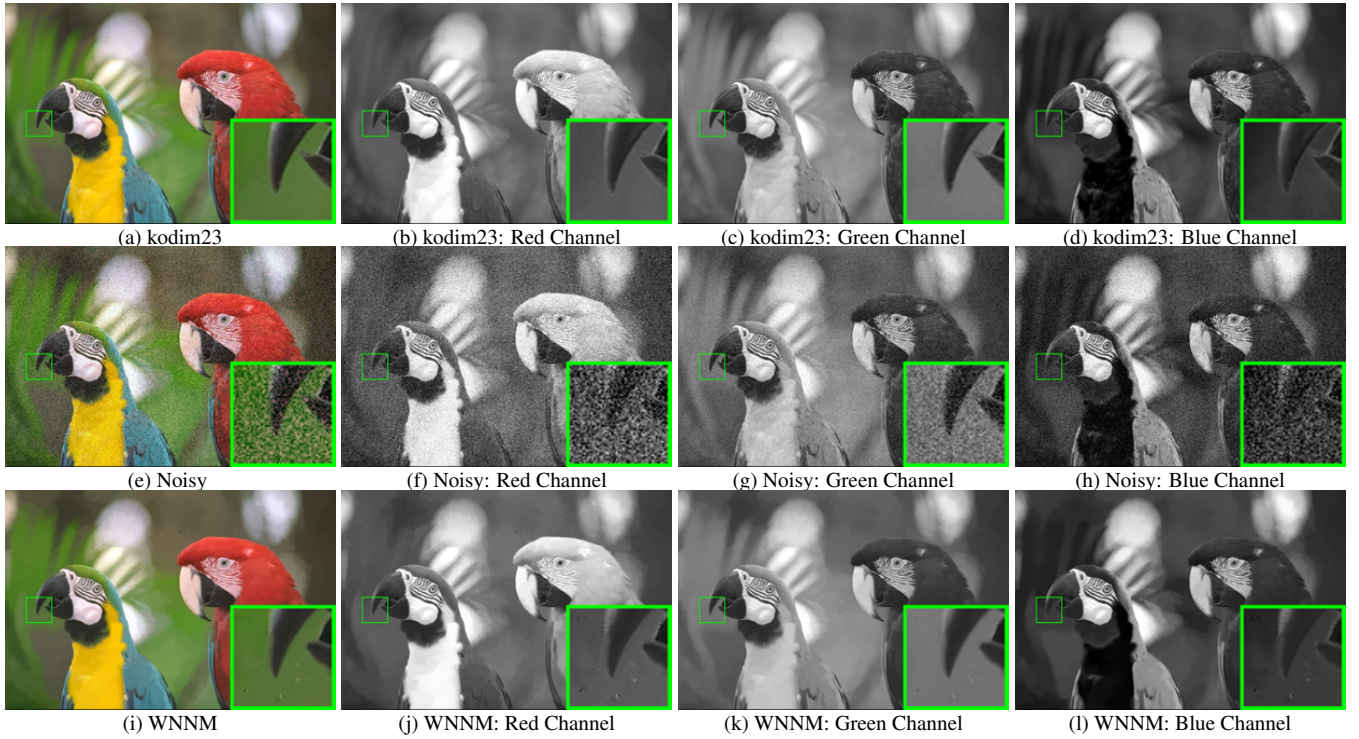


Figure 1. The image “kodim23” of the Kodak PhotoCD dataset, its degraded version, and the image recovered by WNNM. The R, G, B channels are also listed here for image quality comparison.

WNNM method. The weights  $\mathbf{w}$  for the singular values of  $\mathbf{X}$ , then the proposed multi-channel WNNM (MC-WNNM) model is

$$\min_{\mathbf{X}} \|\mathbf{W}(\mathbf{Y} - \mathbf{X})\|_F^2 + \|\mathbf{X}\|_{\mathbf{w},*}. \quad (4)$$

where  $\mathbf{w}$  is the weight vector for singular values of  $\mathbf{X}$ . In [24] and this paper,  $\mathbf{w}$  is set as  $w_i^{k+1} = \frac{C}{|\sigma_i(\mathbf{X}_k)| + \epsilon}$  where  $\epsilon > 0$  is a small number to avoid zero numerator. Note that if  $\sigma_r = \sigma_g = \sigma_b$ , the proposed MC-WNNM model will be reduced to the concatenated WNNM model as a special case. How to set the weighting matrix  $\mathbf{W}$  and how to solve the proposed model will be introduced in the next sections.

### 3.2. The Setting of Weighting Matrix $\mathbf{W}$

For simplicity, in this paper, we assume the noise are independent among the R, G, B channels and i.i.d. in each channel. Assume the noisy patch matrix  $\mathbf{Y} = [\mathbf{Y}_r^\top \mathbf{Y}_g^\top \mathbf{Y}_b^\top]^\top$ , where  $\mathbf{Y}_r, \mathbf{Y}_g, \mathbf{Y}_b$  are matrices of similar patches in R, G, B channels, respectively. The corresponding clean matrix  $\mathbf{X} = [\mathbf{X}_r^\top \mathbf{X}_g^\top \mathbf{X}_b^\top]^\top$ , where  $\mathbf{X}_r, \mathbf{X}_g, \mathbf{X}_b$  are similarly defined. Therefore, the weighting matrix  $\mathbf{W}$  is diagonal and can be determined under the Bayesian framework:

$$\begin{aligned} \hat{\mathbf{X}} &= \arg \max_{\mathbf{X}} \ln P(\mathbf{X} | \mathbf{Y}, \mathbf{w}) \\ &= \arg \max_{\mathbf{X}} \{\ln P(\mathbf{Y} | \mathbf{X}) + \ln P(\mathbf{X} | \mathbf{w})\}. \end{aligned} \quad (5)$$

The log-likelihood term  $\ln P(\mathbf{Y} | \mathbf{X})$  is characterized by the statistics of noise, which is assumed to be channel-wise independent white Gaussian with standard deviations  $\{\sigma_r, \sigma_g, \sigma_b\}$

$$P(\mathbf{Y} | \mathbf{X}) = \prod_{c \in \{r, g, b\}} (2\pi\sigma_c^2)^{-\frac{3p^2}{2}} \exp\left(-\frac{1}{2\sigma_c^2} \|\mathbf{Y}_c - \mathbf{X}_c\|_F^2\right). \quad (6)$$

We assume that the matrix  $\mathbf{X}$  follows the following distribution

$$P(\mathbf{X} | \mathbf{w}) \propto \exp\left(-\frac{1}{2} \|\mathbf{X}\|_{\mathbf{w},*}\right). \quad (7)$$

Putting (7) and (6) into (5), we have

$$\begin{aligned} \hat{\mathbf{X}} &= \arg \min_{\mathbf{X}} \sum_{c \in \{r, g, b\}} \frac{1}{\sigma_c^2} \|(\mathbf{Y}_c - \mathbf{X}_c)\|_F^2 + \|\mathbf{X}\|_{\mathbf{w},*} \\ &= \arg \min_{\mathbf{X}} \|\mathbf{W}(\mathbf{Y} - \mathbf{X})\|_F^2 + \|\mathbf{X}\|_{\mathbf{w},*}, \end{aligned} \quad (8)$$

where

$$\mathbf{W} = \begin{pmatrix} \sigma_r^{-1} \mathbf{I} & \mathbf{0} & \mathbf{0} \\ \mathbf{0} & \sigma_g^{-1} \mathbf{I} & \mathbf{0} \\ \mathbf{0} & \mathbf{0} & \sigma_b^{-1} \mathbf{I} \end{pmatrix}. \quad (9)$$

where  $\mathbf{I} \in \mathbb{R}^{p^2 \times p^2}$  is the identity matrix. Hence, the weighting matrix  $\mathbf{W}$  is determined to contribute equal weights for the pixel values in the same channel, while different weights for those in different channels. The experimental (which will be introduced later) results have already demonstrated

324  
**Algorithm 1:** Color Image Denoising by MC-WNNM  
325   **Input:** Noisy image  $\mathbf{y}$ , noise levels  $\{\sigma_r, \sigma_g, \sigma_b\}$ ;  
326   **Initialization:**  $\hat{\mathbf{x}}^{(0)} = \mathbf{y}, \mathbf{y}^{(0)} = \mathbf{y}$ ;  
327   **for**  $k = 1 : K_1$  **do**  
328     1. Set  $\mathbf{y}^{(k)} = \hat{\mathbf{x}}^{(k-1)}$ ;  
329     2. Extract local patches  $\{\mathbf{y}_j\}_{j=1}^N$  from  $\mathbf{y}^{(k)}$ ;  
330       **for** each patch  $\mathbf{y}_j$  **do**  
331         3. Search non-local similar patches  $\mathbf{Y}_j$ ;  
332         4. Apply the MC-WNNM model (??) to  $\mathbf{Y}_j$  and  
333           obtain the estimated  $\mathbf{X}_j$ ;  
334       **end for**  
335     5. Aggregate  $\{\mathbf{X}_j\}_{j=1}^N$  to form the image  $\hat{\mathbf{x}}^{(k)}$ ;  
336   **end for**  
337   **Output:** Denoised image  $\hat{\mathbf{x}}^{K_1}$ .

---

340 that this form of weighting matrix have already generated  
341 the best denoising performance on synthetic and real noisy  
342 images in benchmark datasets.

### 3.3. The Denoising Algorithm

345 The multi-channel WNNM is applied to the noisy patch  
346 matrix  $\mathbf{Y}_j$  of each local patch  $\mathbf{y}_j$  in the noisy image  $\mathbf{y}$ . And  
347 then all the patches are aggregated together to form the final  
348 recovered image  $\hat{\mathbf{y}}$ . To obtain better denoising results,  
349 we perform the above denoising procedure for several ( $K_1$ )  
350 iterations. The proposed MC-WNNM denoising algorithm  
351 for color images is summarized in Algorithm 1.

### 3.4. Optimization

354 The proposed MC-WNNM model could not be solved  
355 in an analytical form while the original WNNM model  
356 [24] could. In the WNNM model, when the weights on  
357 singular values are non-descending, the weighted nuclear  
358 norm proximal operator [24] can have global optimum with  
359 closed-form solution. However, such property is not valid  
360 for the multi-channel WNNM model. The reason is that the  
361 weighting matrix  $\mathbf{W}$  is added to the rows of matrix  $\mathbf{X}$  instead  
362 of its singular values. Besides, the elements in  $\mathbf{W}$  is  
363 not in a non-descending order with respect to the singular  
364 value of  $\mathbf{X}$ . This makes the proposed model more difficult  
365 to solve when compared to the original WNNM model.

366 By introducing an augmented variable  $\mathbf{Z}$ , the MC-  
367 WNNM model is reformulated as a linear equality-  
368 constrained problem with two variables  $\mathbf{X}$  and  $\mathbf{Z}$ :

$$\min_{\mathbf{X}, \mathbf{Z}} \|\mathbf{W}(\mathbf{Y} - \mathbf{X})\|_F^2 + \|\mathbf{Z}\|_{w,*} \quad \text{s.t. } \mathbf{X} = \mathbf{Z}. \quad (10)$$

371 Since the objective function is separable across the two variables,  
372 the problem (10) can be solved under alternating direction method of multipliers (ADMM) framework. We can  
373 derive its augmented Lagrangian function:  
374

$$\begin{aligned} \mathcal{L}(\mathbf{X}, \mathbf{Z}, \mathbf{A}, \rho) = & \|\mathbf{W}(\mathbf{Y} - \mathbf{X})\|_F^2 + \|\mathbf{Z}\|_{w,*} \\ & + \langle \mathbf{A}, \mathbf{X} - \mathbf{Z} \rangle + \frac{\rho}{2} \|\mathbf{X} - \mathbf{Z}\|_F^2 \end{aligned} \quad (11)$$

375 where  $\mathbf{A}$  is the augmented Lagrangian multiplier and  $\rho > 0$   
376 is the penalty parameter. We initialize the matrix variables  
377  $\mathbf{X}_0, \mathbf{Z}_0$ , and  $\mathbf{A}_0$  to be zero matrix of suitable size. By taking  
378 derivative of the Lagrangian function  $\mathcal{L}$  with respect to the variables  $\mathbf{X}$  and  $\mathbf{Z}$  and setting the derivative function to  
379 be zero, we can alternatively update the ADMM algorithm  
380 iteratively as follows:

381 (1) **Update  $\mathbf{X}$  while fixing  $\mathbf{Z}$  and  $\mathbf{A}$ :**

$$\mathbf{X}_{k+1} = \arg \min_{\mathbf{X}} \|\mathbf{W}(\mathbf{Y} - \mathbf{X})\|_F^2 + \frac{\rho_k}{2} \|\mathbf{X} - \mathbf{Z}_k + \rho_k^{-1} \mathbf{A}_k\|_F^2 \quad (12)$$

385 This is a standard least squares regression problem with  
386 closed-form solution:

$$\mathbf{X}_{k+1} = (\mathbf{W}^\top \mathbf{W} + \frac{\rho_k}{2} \mathbf{I})^{-1} (\mathbf{W}^\top \mathbf{W} \mathbf{Y} + \frac{\rho_k}{2} \mathbf{Z}_k - \frac{1}{2} \mathbf{A}_k) \quad (13)$$

389 (2) **Update  $\mathbf{Z}$  while fixing  $\mathbf{X}$  and  $\mathbf{A}$ :**

$$\mathbf{Z}_{k+1} = \arg \min_{\mathbf{Z}} \frac{\rho_k}{2} \|\mathbf{Z} - (\mathbf{X}_{k+1} + \rho_k^{-1} \mathbf{A}_k)\|_F^2 + \|\mathbf{Z}\|_{w,*} \quad (14)$$

390 According to the Theorem 1 in [24], given the  $\mathbf{X}_{k+1} + \rho_k^{-1} \mathbf{A}_k = \mathbf{U}_k \Sigma_k \mathbf{V}_k^\top$  be the SVD of  $\mathbf{X}_{k+1} + \rho_k^{-1} \mathbf{A}_k$ ,  
391 where  $\Sigma_k = \begin{pmatrix} \text{diag}(\sigma_1, \sigma_2, \dots, \sigma_n) \\ \mathbf{0} \end{pmatrix} \in \mathbb{R}^{m \times n}$ , then the  
392 global optimum of the above problem is  $\hat{\mathbf{Z}} = \mathbf{U}_k \hat{\Sigma}_k \mathbf{V}_k^\top$ ,  
393 where  $\hat{\Sigma}_k = \begin{pmatrix} \text{diag}(\hat{\sigma}_1, \hat{\sigma}_2, \dots, \hat{\sigma}_n) \\ \mathbf{0} \end{pmatrix} \in \mathbb{R}^{m \times n}$  and  
394  $(\hat{\sigma}_1, \hat{\sigma}_2, \dots, \hat{\sigma}_n)$  is the solution to the following convex optimization problem:

$$\begin{aligned} \min_{\hat{\sigma}_1, \hat{\sigma}_2, \dots, \hat{\sigma}_n} & \sum_{i=1}^n (\sigma_i - \hat{\sigma}_i)^2 + \frac{2w_i}{\rho_k} \hat{\sigma}_i \\ \text{s.t. } & \hat{\sigma}_1 \geq \hat{\sigma}_2 \geq \dots \geq \hat{\sigma}_n \geq 0. \end{aligned} \quad (15)$$

408 According to the Remark 1 in [24], the problem above has  
409 closed-form solution

$$\hat{\sigma}_i = \begin{cases} 0 & \text{if } c_2 < 0 \\ \frac{c_1 + \sqrt{c_2}}{2} & \text{if } c_2 \geq 0 \end{cases} \quad (16)$$

410 where  $c_1 = \sigma_i - \epsilon$ ,  $c_2 = (\sigma_i - \epsilon)^2 - \frac{8C}{\rho_k}$  and  $C$  is set as  
411  $\sqrt{2n}$  by experience in image denoising.

412 (3) **Update  $\mathbf{A}$  while fixing  $\mathbf{X}$  and  $\mathbf{Z}$ :**

$$\mathbf{A}_{k+1} = \mathbf{A}_k + \rho_k (\mathbf{X}_{k+1} - \mathbf{Z}_{k+1}) \quad (17)$$

423 (4) **Update  $\rho_k$ :**  $\rho_{k+1} = \mu * \rho_k$ , where  $\mu > 1$ .

424 The above alternative updating steps are repeated until  
425 the convergence condition is satisfied or the number of  
426 iterations exceeds a preset maximum number, e.g.,  $K_2$ .  
427 The convergence condition of the ADMM algorithm is:  
428  $\|\mathbf{X}_{k+1} - \mathbf{Z}_{k+1}\|_F \leq \text{Tol}$ ,  $\|\mathbf{X}_{k+1} - \mathbf{X}_k\|_F \leq \text{Tol}$ , and  
429  $\|\mathbf{Z}_{k+1} - \mathbf{Z}_k\|_F \leq \text{Tol}$  are simultaneously satisfied, where  
430  $\text{Tol} > 0$  is a small tolerance. We summarize the updating

**Algorithm 2:** Solve MC-WNNM via ADMM

**Input:** Matrices  $\mathbf{Y}$  and  $\mathbf{W}$ ,  $\mu > 1$ ,  $\text{Tol} > 0$ ;

**Initialization:**  $\mathbf{X}_0 = \mathbf{Z}_0 = \mathbf{A}_0 = \mathbf{0}$ ,  $\rho_0 > 0$ ,  $T = \text{False}$ ,  $k = 0$ ;

**While** ( $T == \text{false}$ ) **do**

1. Update  $\mathbf{X}_{k+1}$  as  

$$\mathbf{X}_{k+1} = (\mathbf{W}^\top \mathbf{W} + \frac{\rho_k}{2} \mathbf{I})^{-1} (\mathbf{W}^\top \mathbf{W} \mathbf{Y} + \frac{\rho_k}{2} \mathbf{Z}_k - \frac{1}{2} \mathbf{A}_k)$$
  2. Update  $\mathbf{Z}_{k+1}$  by solving the problem  

$$\min_{\mathbf{Z}} \frac{\rho_k}{2} \|\mathbf{Z} - (\mathbf{X}_{k+1} + \rho_k^{-1} \mathbf{A}_k)\|_F^2 + \|\mathbf{Z}\|_{w,*}$$
  3. Update  $\mathbf{A}_{k+1}$  as  $\mathbf{A}_{k+1} = \mathbf{A}_k + \rho_k (\mathbf{X}_{k+1} - \mathbf{Z}_{k+1})$
  4. Update  $\rho_{k+1} = \mu * \rho_k$ ;
  5.  $k \leftarrow k + 1$ ;

**if** (Convergence conditions are satisfied) or ( $k > K_2$ )

5.  $T \leftarrow \text{True}$

end if

end while

**Output:** Matrices X and Z.

steps in Algorithm 2. The convergence analysis of the proposed Algorithm 2 is given in Theorem 1. Note that since the weighted nuclear norm is non-convex in general, we employ an unbounded sequence of  $\{\rho_k\}$  here to make sure that the Algorithm 2 is convergent.

**Theorem 1.** Assume the weights in  $\mathbf{w}$  are in a non-descending order, the sequence  $\{\mathbf{X}_k\}$ ,  $\{\mathbf{Z}_k\}$ , and  $\{\mathbf{A}_k\}$  generated in Algorithm 1 satisfy:

$$(a) \lim_{k \rightarrow \infty} \|\mathbf{X}_{k+1} - \mathbf{Z}_{k+1}\|_F = 0; \quad (18)$$

$$(b) \lim_{k \rightarrow \infty} \|\mathbf{X}_{k+1} - \mathbf{X}_k\|_F = 0; \quad (19)$$

$$(c) \lim_{k \rightarrow \infty} \|\mathbf{Z}_{k+1} - \mathbf{Z}_k\|_F = 0. \quad (20)$$

*Proof.* We give proof sketch here and detailed proof of this theorem can be found in supplementary files. We can first proof that the sequence  $\{\mathbf{A}_k\}$  generated by Algorithm 3.4 is upper bounded. Since  $\{\rho_k\}$  is unbounded, that is  $\lim_{k \rightarrow \infty} \rho_k = +\infty$ , we can proof that the sequence of Lagrangian function  $\{\mathcal{L}(\mathbf{X}_{k+1}, \mathbf{Z}_{k+1}, \mathbf{A}_k, \rho_k)\}$  is also upper bounded. Hence, both  $\{\mathbf{W}(\mathbf{Y} - \mathbf{X}_k)\}$  and  $\{\mathbf{Z}_k\}$  are upper bounded. According to Eq. (17), we can proof that  $\lim_{k \rightarrow \infty} \|\mathbf{X}_{k+1} - \mathbf{Z}_{k+1}\|_F = \lim_{k \rightarrow \infty} \rho_k^{-1} \|\mathbf{A}_{k+1} - \mathbf{A}_k\|_F = 0$ , and (a) is proofed. Then we can proof that  $\lim_{k \rightarrow \infty} \|\mathbf{X}_{k+1} - \mathbf{X}_k\|_F \leq \lim_{k \rightarrow \infty} \|(\mathbf{W}^\top \mathbf{W} + \frac{\rho_k}{2} \mathbf{I})^{-1} (\mathbf{W}^\top \mathbf{W} \mathbf{Y} - \mathbf{W}^\top \mathbf{W} \mathbf{Z}_k - \frac{1}{2} \mathbf{A}_k)\|_F + \rho_k^{-1} \|\mathbf{A}_k - \mathbf{A}_{k-1}\|_F = 0$  and hence (b) is proofed. Then (c) can be proofed by checking that  $\lim_{k \rightarrow \infty} \|\mathbf{Z}_{k+1} - \mathbf{Z}_k\| \leq \lim_{k \rightarrow \infty} \|\Sigma_{k-1} - \mathcal{S}_{w/\rho_{k-1}}(\Sigma_{k-1})\|_F + \|\mathbf{X}_{k+1} - \mathbf{X}_k\|_F + \rho_k^{-1} \|\mathbf{A}_{k-1} + \mathbf{A}_{k+1} - \mathbf{A}_k\|_F = 0$ , where  $\mathbf{U}_{k-1} \Sigma_{k-1} \mathbf{V}_{k-1}^\top$  is the SVD of the matrix  $\mathbf{X}_k + \rho_{k-1} \mathbf{A}_{k-1}$ .  $\square$

## 4. Experiments

We evaluate the proposed MC-WNNM method on synthetic and real color image denoising. We compare the proposed method with other state-of-the-art denoising methods including CBM3D [17], MLP [10], WNNM [7], TNRD [12], “Noise Clinic” (NC) [19, 26], and the commercial software Neat Image (NI) [28].

#### **4.1. Implementation Details**

In synthetic experiments, the noise levels in R, G, B channels are assumed to be known as  $\sigma_r, \sigma_g, \sigma_b$ . In the real cases, the noise levels in R, G, B channels can be estimated via noise estimation methods [29, 30]. In this paper, we employ the method of [30] for its state-of-the-art performance. For the CBM3D method [17], the input noise levels are the Root Mean Square (RMS) as

$$\sigma = \sqrt{(\sigma_r^2 + \sigma_g^2 + \sigma_b^2)/3}. \quad (21)$$

For the methods of MLP [10] and TNRD [12], we retrain the models on grayscale images following their corresponding strategies at different noise levels from  $\sigma = 5$  to  $\sigma = 75$  with gap of 5. The denoising on color images is performed by processing separately each channel with the model trained at the same (or nearest) noise levels. NC [19, 26] is a blind image denoising method, so we just submit the noisy images (synthetic or real) to [26] and perform denoising using the default parameters. NI [28] is a commercial software suitable for real image denoising, while the code of CC [14] is not released (but its results on the 15 real noisy images in [14] are available by requesting the authors). Hence, we only compare with CC and NI in real image denoising experiments, and do not compare with them in synthetic experiments.

In order to take fully comparison with the original WNNM method [24], we extended the WNNM method [24] for color image denoising in three directions: 1) we apply the WNNM method [24] on each channel separately with corresponding noise levels  $\sigma_r, \sigma_g, \sigma_b$ . We call this method “WNNM0”; 2) we perform denoising on the joint vectors concatenated by corresponding patches in the R, G, B channels, where the input noise level  $\sigma$  is computed by RMS (Eq. (21)). We call this method “WNNM1”; 3) we set the weighting matrix  $\mathbf{W}$  in the proposed MC-WNNM model as  $\mathbf{W} = \sigma^{-1} \mathbf{I}$ . For fair comparison, we tune all these methods set the same parameters for “WNNM2” and the proposed MC-WNNM methods while achieving the best performance of “WNNM2”. For fair comparison, we tune the methods of “WNNM0”, “WNNM1”, “WNNM2”, and the proposed MC-WNNM to achieve corresponding best denoising performance (i.e., highest average PSNR results).

540

## 4.2. Experiments on Synthetic Noisy Images

In this section, we compare the proposed MC-WNNM method with other competing denoising methods [10, 12, 17, 19, 28] as well as the three extensions of the original WNNM method [24] on the 24 high quality color images from the Kodak PhotoCD Dataset (<http://r0k.us/graphics/kodak/>), which are shown in Fig. 2. The noisy images are generated by adding additive white Gaussian noise (AWGN) with known standard derivations  $\sigma_r, \sigma_g, \sigma_b$  for the R, G, B channels, respectively. In this paper, the noise levels we add to each channel of the 24 color images are  $\sigma_r = 40, \sigma_g = 20, \sigma_b = 30$ , respectively. More experiments can be found in the supplementary files. For the methods of “WNNM2” and MC-WNNM, we set the patch size as  $p = 6$ , the number of non-local similar patches as  $M = 70$ , the window size for searching similar patches as  $W = 20$ , the updating parameter  $\mu = 1.001$ , the number of iterations in Algorithm 1 as  $K_1 = 8$ , the number of iterations in Algorithm 2 as  $K_2 = 10$ . For “WNNM2”, the initial penalty parameter is set as  $\rho_0 = 10$ , while for the proposed MC-WNNM model, the penalty parameter is set as  $\rho_0 = 3$ .

The PSNR results are listed in Table 1 of the compared methods including CBM3D [17], MLP [10], TNRD [12], NI [28], NC [19, 26], “WNNM0” [24], “WNNM1”, “WNNM2” and the proposed MC-WNNM methods. The best PSNR results are highlighted in bold. One can see that on all the 24 images, our method achieves the highest PSNR values over the competing methods. On average PSNR, our proposed method achieves 0.48dB improvements over the “WNNM0” method and outperforms the “WNNM2” by 1.09dB. Fig. 3 shows a scene denoised by the compared methods. We can see that the methods of CBM3D and NC would remain some noise on the recovered images. The methods of MLP, TNRD, and “WNNM0”, which process separately the channels of color images, would over-smooth the images and generate false colors or artifacts. The method “WNNM1”, which process jointly the channels of color images, would not generate false colors, but still over-smooth the image. The “WNNM2”, which is the WNNM model solved by ADMM algorithm, would remain some noise on the image. By employing the proposed MC-WNNM model, our method preserves the structures (e.g., textures in windows and grass) better across the R, G, B channels and generate less artifacts than other denoising methods, leading to visually pleasant outputs. More visual comparisons can be found in the supplementary files.

## 4.3. Experiments on Real Noisy Images

In this section, we compare the proposed MC-WNNM method with other competing methods on the 15 real noisy images (Fig. 4). We do not compare with the “WNNM0” method due to limited space and its inferior performance.



Figure 2. The 24 high quality color images from the Kodak PhotoCD Dataset.

The noisy images were collected under controlled indoor environment. Each scene was shot 500 times under the same camera and camera setting. The mean image of the 500 shots is roughly taken as the “ground truth”, with which the PSNR can be computed. Since the image size is very large (about  $7000 \times 5000$ ) and the 11 scenes share repetitive contents, the authors of [14] cropped 15 smaller images (of size  $512 \times 512$ ) to perform experiments. For each real noisy image, the noise levels in R, G, B channels are estimated by [30]. Since the noise levels are small in real noisy images, for the method of MLP [10] and TNRD [12], we apply the trained models of corresponding methods and choose the best denoising results (highest average PSNR values). Both methods achieve best results when setting the noise levels of the trained models from  $\sigma = 10$ .

We perform quantitative comparison on the 15 cropped images used in [14]. The PSNR results are listed in Table 2 of the compared methods including CBM3D [17], MLP [10], TNRD [12], NC [19, 26], NI [28], CC [14] (copied from [14]), “WNNM1”, “WNNM2”, and the proposed MC-WNNM method. The highest PSNR results are highlighted in bold. On average PSNR, the proposed MC-WNNM method achieves 0.44dB improvements over the “WNNM1” method and outperforms the state-of-the-art denoising method CC [14] by 0.83dB. On 10 out of the whole 15 images, the proposed MC-WNNM method achieves the highest PSNR values. Both CC and “WNNM1” achieves highest PSNR results on 2 of 15 images. It should be noted that in the CC method, a specific model is trained for each camera and camera setting, while our method uses the same model for all cases. Fig. 5 shows the denoised images of a scene captured by Canon 5D Mark 3 at ISO = 3200. We can see that CBM3D, NC, NI and CC would either remain noise or generate artifacts, while TNRD, “WNNM1”, and “WNNM2” over-smooth much the image. By using the proposed MC-WNNM model achieves better visual quality results than other methods. More visual comparisons can be found in the supplementary files.

648

649

650

651

652

653

654

655

656

657

658

659

660

661

662

663

664

665

666

667

668

669

670

671

672

673

674

675

676

677

678

679

680

681

682

683

684

685

686

687

688

689

690

691

692

693

694

695

696

697

698

699

700

701

702

703

704

705

706

707

708

709

710

711

712

713

714

715

716

717

718

719

720

721

722

723

724

725

726

727

728

729

730

731

732

733

734

735

736

737

738

739

740

741

742

743

744

745

746

747

748

749

750

751

752

753

754

755

Table 1. PSNR(dB) results of different denoising algorithms on 24 natural images.

Image#	$\sigma_r = 40, \sigma_g = 20, \sigma_b = 30$								
	CBM3D	MLP	TNRD	NI	NC	WNNM0	WNNM1	WNNM2	MC-WNNM
1	25.24	25.70	25.74	23.85	24.90	26.01	25.95	25.58	<b>26.66</b>
2	28.27	30.12	30.21	25.90	25.87	30.08	30.11	29.80	<b>30.20</b>
3	28.81	31.19	31.49	26.00	28.58	31.58	31.61	31.20	<b>32.25</b>
4	27.95	29.88	29.86	25.82	25.67	30.13	30.16	29.84	<b>30.49</b>
5	25.03	26.00	26.18	24.38	25.15	26.44	26.39	25.32	<b>26.82</b>
6	26.24	26.84	26.90	24.65	24.74	27.39	27.30	26.88	<b>27.98</b>
7	27.88	30.28	30.40	25.63	27.69	30.47	30.54	29.70	<b>30.98</b>
8	25.05	25.59	25.83	24.02	25.30	26.71	26.75	25.26	<b>26.90</b>
9	28.44	30.75	30.81	25.94	27.44	30.86	30.92	30.29	<b>31.49</b>
10	28.27	30.38	30.57	25.87	28.42	30.65	30.68	29.95	<b>31.26</b>
11	26.95	28.00	28.14	25.32	24.67	28.19	28.16	27.61	<b>28.63</b>
12	28.76	30.87	31.05	26.01	28.37	30.97	31.06	30.58	<b>31.48</b>
13	23.76	23.95	23.99	23.53	22.76	24.27	24.15	23.52	<b>24.89</b>
14	26.02	26.97	27.11	24.94	25.68	27.20	27.15	26.55	<b>27.57</b>
15	28.38	30.15	30.44	26.06	28.21	30.52	30.60	30.13	<b>30.81</b>
16	27.75	28.82	28.87	25.69	26.66	29.27	29.21	29.02	<b>29.96</b>
17	27.90	29.57	29.80	25.85	28.32	29.78	29.79	29.16	<b>30.40</b>
18	25.77	26.40	26.41	24.74	25.70	26.63	26.56	26.01	<b>27.22</b>
19	27.30	28.67	28.81	25.40	26.52	29.19	29.22	28.67	<b>29.57</b>
20	28.96	30.40	30.76	24.95	25.90	30.79	30.83	29.97	<b>31.07</b>
21	26.54	27.53	27.60	25.06	26.48	27.80	27.75	27.12	<b>28.34</b>
22	27.05	28.17	28.27	25.36	26.60	28.21	28.16	27.81	<b>28.64</b>
23	29.14	32.31	32.51	26.13	23.24	31.89	31.97	31.21	<b>32.34</b>
24	25.75	26.41	26.53	24.55	25.73	27.10	27.03	26.18	<b>27.59</b>
Average	27.13	28.54	28.68	25.24	26.19	28.84	28.83	28.22	<b>29.31</b>

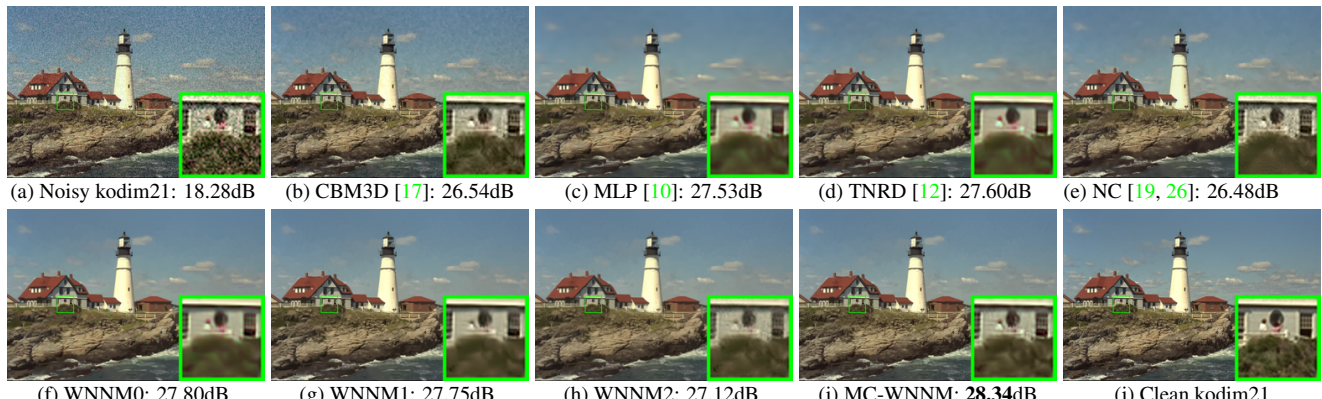
Figure 3. Denoised images of different methods on the image "kodim21" degraded by AWGN with different standard derivations of  $\sigma_r = 40, \sigma_g = 20, \sigma_b = 30$  on R, G, B channels, respectively. The images are better to be zoomed in on screen.

Figure 4. The 15 cropped real noisy images used in [14].

## 5. Conclusion and Future Work

The real noisy images have different noise structures among the R, G, B channels due to the preprocessing steps

of the digital camera pipelines in CCD or CMOS sensors. This makes the real image denoising problem much more complex than grayscale image denoising. In this paper, we proposed a novel multi-channel (MC) model for real color image denoising. By introducing a weighting matrix to the concatenated weighted nuclear norm minimization (WNNM) model, the proposed MC-WNNM model can process adaptively the different noise structures in each of the R, G, B channels and exploit the non-local self similarity property of natural images. Though no longer having closed-form solution, we successfully solved the MC-WNNM model via an ADMM algorithm by reformulating the MC-WNNM model as a linear equality-constrained problem with two separable variables. We also studied the convergence property of the ADMM algorithm. Extensive experiments on synthetic and real color image denois-

Table 2. PSNR(dB) results of different methods on 15 cropped real noisy images used in [14].

Camera Settings	CBM3D	MLP	TNRD	NI	NC	CC	WNNM1	WNNM2	MC-WNNM
Canon 5D Mark III ISO = 3200	39.76 36.40 36.37	39.00 36.34 36.33	39.51 36.47 36.45	35.68 34.03 32.63	36.20 34.35 33.10	38.37 35.37 34.91	39.74 35.12 33.14	39.98 36.65 34.63	<b>41.13</b> <b>37.28</b> <b>36.52</b>
Nikon D600 ISO = 3200	34.18 35.07 37.13	34.70 36.20 39.33	34.79 36.37 39.49	31.78 35.16 39.98	32.28 35.34 40.51	34.98 35.95 <b>41.15</b>	35.08 36.42 40.78	35.08 36.84 39.24	<b>35.53</b> <b>37.02</b> 39.56
Nikon D800 ISO = 1600	36.81 37.76 37.51	37.95 40.23 37.94	38.11 40.52 38.17	34.84 38.42 35.79	35.09 38.65 35.85	37.99 40.36 38.30	38.28 41.24 38.04	38.61 40.81 38.96	<b>39.26</b> <b>41.43</b> <b>39.55</b>
Nikon D800 ISO = 3200	35.05 34.07 34.42	37.55 35.91 38.15	37.69 35.90 38.21	38.36 35.53 40.05	38.56 35.76 40.59	<b>39.01</b> 36.75 39.06	39.93 37.32 41.52	37.97 37.30 38.68	38.91 <b>37.41</b> 39.39
Nikon D800 ISO = 6400	31.13 31.22 30.97	32.69 32.33 32.29	32.81 32.33 32.29	34.08 32.13 31.52	34.25 32.38 31.76	34.61 33.21 33.22	35.20 33.61 33.62	34.57 33.43 34.02	34.80 <b>33.95</b> 33.94
Average	35.19	36.46	36.61	35.33	35.65	36.88	37.27	37.12	<b>37.71</b>

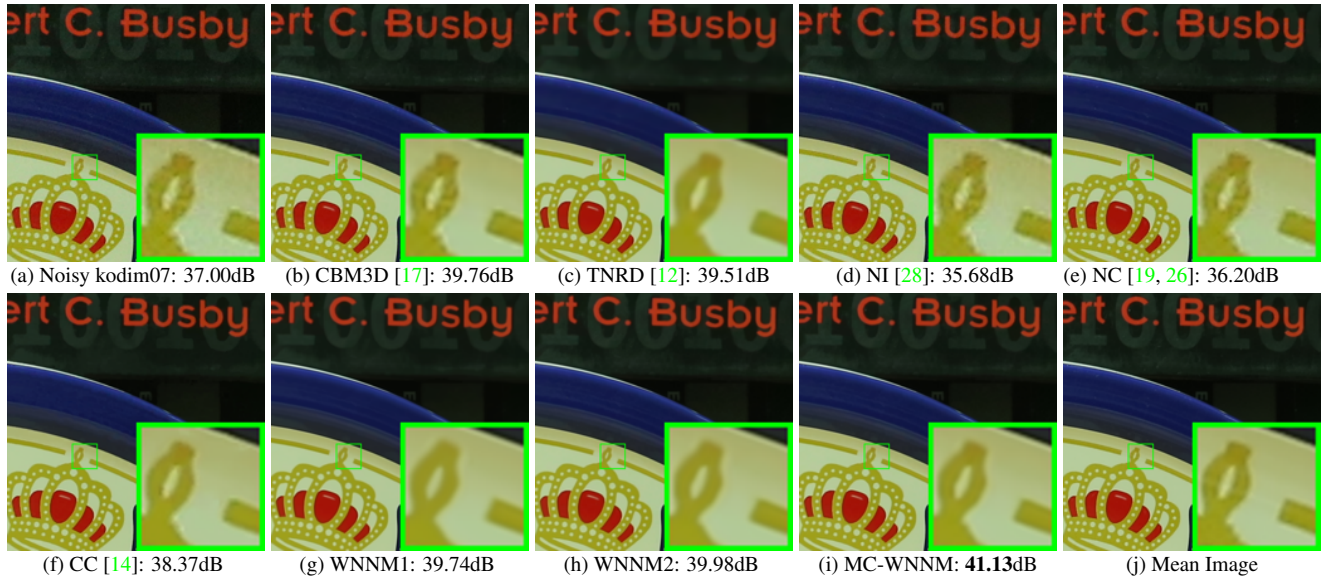


Figure 5. Denoised images of a region cropped from the real noisy image “Canon 5D Mark 3 ISO 3200 1” [14] by different methods. The images are better to be zoomed in on screen.

ing demonstrate that, the proposed MC-WNNM model outperforms the other competing denoising methods on both synthetic color noisy images as well as real-world noisy images. Introducing a weighting matrix to the traditional models for grayscale image denoising can boost the performance of traditional models on color image denoising tasks. We believe that this work can be extended in at least two directions. Firstly, the weighting matrix beyond the diagonal form, such as correlation form [31], may bring better performance on color image denoising. Secondly, the proposed MC-WNNM model can be further extended to deal

with hyperspectral images, which may contain hundreds of channels (bands) with different noise structures in different channels.

## References

- [1] A. Buades, B. Coll, and J. M. Morel. A non-local algorithm for image denoising. *IEEE Conference on Computer Vision and Pattern Recognition (CVPR)*, pages 60–65, 2005. **1**
- [2] K. Dabov, A. Foi, V. Katkovnik, and K. Egiazarian. Image denoising by sparse 3-D transform-domain collabora-

- 864      tive filtering. *IEEE Transactions on Image Processing*,  
865      16(8):2080–2095, 2007. 1, 2
- 866
- 867 [3] M. Elad and M. Aharon. Image denoising via sparse  
868 and redundant representations over learned dictionaries.  
869 *IEEE Transactions on Image Processing*, 15(12):3736–3745,  
870 2006.
- 871 [4] J. Mairal, F. Bach, J. Ponce, G. Sapiro, and A. Zisserman.  
872 Non-local sparse models for image restoration. *IEEE International  
873 Conference on Computer Vision (ICCV)*, pages  
874 2272–2279, 2009.
- 875 [5] W. Dong, L. Zhang, G. Shi, and X. Li. Nonlocally central-  
876 ized sparse representation for image restoration. *IEEE Trans-  
877 actions on Image Processing*, 22(4):1620–1630, 2013.
- 878 [6] J. Xu, L. Zhang, W. Zuo, D. Zhang, and X. Feng. Patch  
879 group based nonlocal self-similarity prior learning for image  
880 denoising. *IEEE International Conference on Computer Vi-  
881 sion (ICCV)*, pages 244–252, 2015.
- 882 [7] S. Gu, L. Zhang, W. Zuo, and X. Feng. Weighted nu-  
883 clear norm minimization with application to image denois-  
884 ing. *IEEE Conference on Computer Vision and Pattern  
885 Recognition (CVPR)*, pages 2862–2869, 2014. 1, 2, 5
- 886 [8] S. Roth and M. J. Black. Fields of experts. *International  
887 Journal of Computer Vision*, 82(2):205–229, 2009. 1
- 888 [9] D. Zoran and Y. Weiss. From learning models of natural  
889 image patches to whole image restoration. *IEEE Interna-  
890 tional Conference on Computer Vision (ICCV)*, pages 479–  
891 486, 2011.
- 892 [10] H. C. Burger, C. J. Schuler, and S. Harmeling. Image de-  
893 noising: Can plain neural networks compete with BM3D?  
894 *IEEE Conference on Computer Vision and Pattern Recog-  
895 nition (CVPR)*, pages 2392–2399, 2012. 5, 6, 7
- 896 [11] U. Schmidt and S. Roth. Shrinkage fields for effective im-  
897 age restoration. *IEEE Conference on Computer Vision and  
898 Pattern Recognition (CVPR)*, pages 2774–2781, June 2014.
- 899 [12] Y. Chen, W. Yu, and T. Pock. On learning optimized re-  
900 action diffusion processes for effective image restoration.  
901 *IEEE Conference on Computer Vision and Pattern Recog-  
902 nition (CVPR)*, pages 5261–5269, 2015. 1, 5, 6, 7, 8
- 903 [13] B. Leung, G. Jeon, and E. Dubois. Least-squares luma-  
904 chroma demultiplexing algorithm for bayer demosaicking.  
905 *IEEE Transactions on Image Processing*, 20(7):1885–1894,  
906 2011. 1, 2
- 907 [14] S. Nam, Y. Hwang, Y. Matsushita, and S. J. Kim. A holistic  
908 approach to cross-channel image noise modeling and its ap-  
909 plication to image denoising. *IEEE Conference on Computer  
910 Vision and Pattern Recognition (CVPR)*, pages 1683–1691,  
911 2016. 1, 2, 5, 6, 7, 8
- 912 [15] H. C. Karaimer and M. S. Brown. A software platform for  
913 manipulating the camera imaging pipeline. *European Con-  
914 ference on Computer Vision (ECCV)*, October 2016. 1
- 915 [16] Julien Mairal, Michael Elad, and Guillermo Sapiro. Sparse  
916 representation for color image restoration. *IEEE Transac-  
917 tions on Image Processing*, 17(1):53–69, 2008. 1, 2
- 918 [17] K. Dabov, A. Foi, V. Katkovnik, and K. Egiazarian. Color  
919 image denoising via sparse 3D collaborative filtering with  
920 grouping constraint in luminance-chrominance space. *IEEE  
921 International Conference on Image Processing (ICIP)*, pages  
922 313–316, 2007. 1, 2, 5, 6, 7, 8
- 923 [18] C. Liu, R. Szeliski, S. Bing Kang, C. L. Zitnick, and W. T.  
924 Freeman. Automatic estimation and removal of noise from  
925 a single image. *IEEE Transactions on Pattern Analysis and  
926 Machine Intelligence*, 30(2):299–314, 2008. 1, 2
- 927 [19] M. Lebrun, M. Colom, and J.-M. Morel. Multiscale image  
928 blind denoising. *IEEE Transactions on Image Processing*,  
929 24(10):3149–3161, 2015. 1, 2, 5, 6, 7, 8
- 930 [20] F. Zhu, G. Chen, and P.-A. Heng. From noise modeling to  
931 blind image denoising. *IEEE Conference on Computer Vi-  
932 sion and Pattern Recognition (CVPR)*, June 2016. 1, 2
- 933 [21] S. Boyd, N. Parikh, E. Chu, B. Peleato, and J. Eckstein. Dis-  
934 tributed optimization and statistical learning via the alternat-  
935 ing direction method of multipliers. *Found. Trends Mach.  
936 Learn.*, 3(1):1–122, January 2011. 1
- 937 [22] C. Lu, C. Zhu, C. Xu, S. Yan, and Z. Lin. Generalized sin-  
938 gular value thresholding. *AAAI*, 2015. 1
- 939 [23] J. Cai, E. J. Candès, and Z. Shen. A singular value thresh-  
940 olding algorithm for matrix completion. *SIAM Journal on  
941 Optimization*, 20(4):1956–1982, 2010. 2
- 942 [24] S. Gu, Q. Xie, D. Meng, W. Zuo, X. Feng, and L. Zhang.  
943 Weighted nuclear norm minimization and its applications to  
944 low level vision. *International Journal of Computer Vision*,  
945 pages 1–26, 2016. 2, 3, 4, 5, 6
- 946 [25] C. Eckart and G. Young. The approximation of one matrix by  
947 another of lower rank. *Psychometrika*, 1(3):211–218, 1936.  
948 2
- 949 [26] M. Lebrun, M. Colom, and J. M. Morel. The noise clinic:  
950 a blind image denoising algorithm. [http://www.ipol.  
951 im/pub/art/2015/125/](http://www.ipol.im/pub/art/2015/125/). Accessed 01 28, 2015. 2, 5,  
952 6, 7, 8
- 953 [27] C. Kervrann, J. Boulanger, and P. Coupé. Bayesian non-  
954 local means filter, image redundancy and adaptive dictionar-  
955 ries for noise removal. *International Conference on Scale  
956 Space and Variational Methods in Computer Vision*, pages  
957 520–532, 2007. 2
- 958 [28] Neatlab ABSoft. Neat Image. [https://ni.  
959 neatvideo.com/home](https://ni.neatvideo.com/home). 2, 5, 6, 8
- 960 [29] X. Liu, M. Tanaka, and M. Okutomi. Single-image noise  
961 level estimation for blind denoising. *IEEE Transactions on  
962 Image Processing*, 22(12):5226–5237, 2013. 5
- 963
- 964
- 965
- 966
- 967
- 968
- 969
- 970
- 971

- 972 [30] G. Chen, F. Zhu, and A. H. Pheng. An efficient statistical 1026  
973 method for image noise level estimation. *IEEE International 1027  
974 Conference on Computer Vision (ICCV)*, December 2015. 5, 1028  
975 6 1029  
976 1030  
977 [31] N. J. Higham. Computing the nearest correlation matrixa 1031  
978 problem from finance. *IMA Journal of Numerical Analysis*, 1032  
979 22(3):329, 2002. 8 1033  
980 1034  
981 1035  
982 1036  
983 1037  
984 1038  
985 1039  
986 1040  
987 1041  
988 1042  
989 1043  
990 1044  
991 1045  
992 1046  
993 1047  
994 1048  
995 1049  
996 1050  
997 1051  
998 1052  
999 1053  
1000 1054  
1001 1055  
1002 1056  
1003 1057  
1004 1058  
1005 1059  
1006 1060  
1007 1061  
1008 1062  
1009 1063  
1010 1064  
1011 1065  
1012 1066  
1013 1067  
1014 1068  
1015 1069  
1016 1070  
1017 1071  
1018 1072  
1019 1073  
1020 1074  
1021 1075  
1022 1076  
1023 1077  
1024 1078  
1025 1079